Modeling Io's Sublimation-Driven Atmosphere: Gas Dynamics and Radiation Emission

Andrew C. Walker[†], Sergey L. Gratiy[*], Deborah A. Levin[*], David B. Goldstein[†], Philip L. Varghese[†], Laurence M. Trafton[†], Chris H. Moore[†], Benedicte Stewart[†]

[†]*University of Texas at Austin, Department of Aerospace Engineering, 210 East 24th Street W. R. Woolrich Laboratories 1 University Station, C0600 Austin, TX 78712*
[*]*Pennsylvania State University, Department of Aerospace Engineering, 229 Hammond, University Park, PA 16802*

Abstract. Io's sublimation-driven atmosphere is modeled using the direct simulation Monte Carlo method. These rarefied gas dynamics simulations improve upon earlier models by using a three-dimensional domain encompassing the entire planet computed in parallel. The effects of plasma impact heating, planetary rotation, and inhomogeneous surface frost are investigated. Circumplanetary flow is predicted to develop from the warm subsolar region toward the colder night-side. The non-equilibrium thermal structure of the atmosphere, including vibrational and rotational temperatures, is also presented. Io's rotation leads to an asymmetric surface temperature distribution which is found to strengthen circumplanetary flow near the dusk terminator. Plasma heating is found to significantly inflate the atmosphere on both day- and night-sides. The plasma energy flux also causes high temperatures at high altitudes but permits relatively cooler temperatures at low altitudes near the dense subsolar point due to plasma energy depletion. To validate the atmospheric model, a radiative transfer model was developed utilizing the backward Monte Carlo method. The model allows the calculation of the atmospheric radiation from emitting/absorbing and scattering gas using an arbitrary scattering law and an arbitrary surface reflectivity. The model calculates the spectra in the ν_2 vibrational band of SO_2 which are then compared to the observational data.

Keywords: Io, Atmosphere
PACS: 96.12.Jt, 96.12.Kz, 96.30.lb

INTRODUCTION

There are two important mechanisms on Jupiter's moon Io which could produce an atmosphere: volcanic activity and sublimation from surface frost. Simulations by Saur and Strobel indicate that sublimation is likely the dominant mechanism for creating the day-side atmosphere [1]. They model the interaction of the Jovian plasma torus with the atmosphere, finding that sublimation is roughly 10 times as important in controlling the atmospheric column of SO_2 on the day-side. Therefore, for the present, we only simulate the dominant mechanism for the day-side column, the sublimated flux of SO_2 from the surface frost.

There have been several attempts to model Io's rarefied atmosphere. Ingersoll et al. [2] integrated the conservation equations vertically to find sublimation-driven flow. They assumed turbulent atmospheric flow, negligible effect from planetary rotation, and uniform frost coverage controlled by a surface in blackbody equilibrium with solar radiation. They found that supersonic pressure-driven flow develops as gas sublimates from areas near the warm subsolar region and condenses in the colder regions near the terminator. Similar results were found by Moreno et al. who allowed the atmosphere to vary with altitude and also included a crude radiative transfer model [3]. Both found that the sublimation region extends from the subsolar point to a solar incidence angle $\theta \le 37^o$, where the atmospheric pressure exceeds the vapor pressure of SO_2. Wong and Johnson [4] were the first to compute the effect of plasma bombardment on Io's sublimation atmosphere, which they found to significantly inflate the upper atmosphere. Wong and Johnson [5] later included photochemistry and tracked the daughter species of SO_2, while Wong and Smyth [6] refined the plasma model. These simulations all modeled the atmosphere as a continuum; this is a poor approximation where the atmosphere is rarefied (at high altitudes and away from the subsolar region). Pospieszalska and Johnson used 1-D Monte Carlo calculations to characterize the effect of ion bombardment on the vertical structure and atmospheric loss rate [7]. Austin and Goldstein used the direct simulation

Monte Carlo (DSMC) method to simulate circumplanetary flows [8]. They presented a 2-D axi-symmetric simulation of sublimation/condensation driven flow.

The distribution of SO_2 frost on Io's surface should be closely linked with the surface temperature and the column density. Douté et al. investigated the abundance of SO_2 frost by analyzing images acquired by the Galileo NIMS instrument and found that SO_2 frost deposits cover about three quarters of Io's surface [9]. Frost appears omnipresent over Io's surface but is concentrated within several large areas centered at medium latitudes.

Here we present a fully three-dimensional model of the Io's sublimation atmosphere computed using DSMC. Circumplanetary flow is found to occur due to a pressure gradient (caused by a relatively high vapor pressure on the sunlit side) causing flow away from the subsolar point. The gas densities span the range from collisional (near the subsolar point at low altitudes) to free molecular flow (at high altitudes and on the night-side). Density variations as a function of latitude and longitude are also examined and compared to derived column densities based on recent observations [10]. Our three-dimensional simulation is able to model asymmetries in atmospheric parameters such as density, temperature, and flow velocity due to planetary rotation and an inhomogeneous frost distribution.

MODEL

The range of flow densities on Io fluctuates greatly from ~10^{17} molecule/m^3 near the subsolar point to less than 10^{12} molecule/m^3 on the night-side at high altitudes. The atmosphere on the night-side and everywhere at high altitudes is of such low density that the gas property gradients occur on length scales that are smaller than the mean free path. DSMC is the most suitable choice for modeling such rarefied flow conditions [11].

Our current DSMC code includes many adaptations and modifications of Bird's original DSMC code. The molecules experience a gravitational force and therefore travel along elliptic trajectories between collisions. Rotational energy levels are considered to be continuous while vibrational energy states are discrete due to the relatively cold temperatures in Io's atmosphere; all three modes of vibration are treated for SO_2. The vibrational and rotational states are populated by assuming that sublimated molecules are in thermal equilibrium with the surface. During the gas dynamics calculation, the atmosphere is assumed to be optically thin, so that any radiation emitted from an SO_2 molecule is lost (for details, see [12]). Plasma bombardment by ions, neutrals, and electrons from Jupiter's co-rotating plasma torus is modeled via a plasma energy flux (5.0 mW/m^2). The plasma energy enters radially from the top of the domain and is currently assumed uniform over the entire planet. Excitation of translational and rotational modes by the plasma is accounted for by depositing an equal amount of energy into each degree of freedom while vibrational excitation is rare enough to be neglected. The depletion of plasma energy in a given cell depends on the gas density. The remaining energy travels down a column of cells until it is completely depleted or reaches the surface [8].

The computational model uses a three-dimensional spherical geometry extending from Io's surface to an altitude of 200 km. The upper edge of the domain has a vacuum boundary condition; negligibly few molecules are lost at this boundary. The grid is stretched exponentially in the radial direction to keep the cell height equal to or less than the mean free path. The lower edge of the domain at the surface has a unit sticking coefficient. Molecules which strike the surface have a probability of striking either frost or rock depending on the frost coverage fraction for that surface cell, f_{SO_2}. Near the subsolar point at the surface, the mean free path at a temperature of 120 K is ~1 m, but the mean free path grows exponentially with altitude and solar zenith angle. The cell size at high altitudes is limited to 5 km to remain smaller than the local scale height of the atmosphere. The grid size generally exceeds the mean free path in directions tangent to the surface, but grid convergence studies showed that the length scale of gradients in these directions is appreciably greater than the cell size.

The cell sizes in latitude and longitude have a resolution of 1° (180 × 360 cells). The domain is decomposed in the azimuthal direction between 36 processors, with each processor receiving 10 degrees of longitude. The boundaries between processors are message passing interfaces across which molecules are passed. Each processor simulates 180,000 cells and, for adequate statistics, ~10 molecules per cell are used where there is any gas. The function f_{SO_2} is given with one degree resolution in both latitude and longitude [9]. There were no data available between longitudes of 0° to 90° and at high latitudes, so f_{SO_2} was interpolated using a linear interpolation scheme between 0° to 90° and by hand for high latitudes. Rock and frost covered areas within a pixel are assumed to be discrete; each has its own temperature (T_{frost} and T_{rock}) based on the emissivity of that surface type. The entire surface of Io is assumed to be a gray body, so that the emissivity, e, can be calculated directly from the albedo. The Bond albedo of frost is assumed ~0.8 and of rock ~0.2. The sublimation rate of SO_2, equilibrium vapor pressure, and the surface temperature are given by

$$N_{sub} = \frac{P_{vap}}{\sqrt{2\pi k_B T_s M_{SO_2}}} \cdot f_{SO_2} \qquad P_{vap} = 1.516\times10^{13} e^{\frac{-4510}{T_{frost}}} \qquad \frac{dT_s}{dt} = \begin{cases} \frac{e\sigma}{Mc}\left(T_{\min}^4 - T_s^4\right) \rightarrow \text{nightside} \\ \frac{e\sigma}{Mc}\left(T_{ss}^4 - T_s^4\right) \rightarrow \text{dayside} \end{cases} \quad (1.1)$$

where σ is the Stefan-Boltzmann constant, T_{min} is the anti-solar temperature (90 K [14]), T_{ss} is the subsolar temperature (120 K), and Mc = 182 J/m^2-K is a thermal parameter (the same for rock and frost) derived from observed 20 and 30 μm radiance data [1]. The planetary rotation of Io is included through the temperature distribution model.

The frost fraction is also used to determine the probability of a molecule landing on rock or frost. If a molecule lands on a frost covered surface, it is deleted from the computation, because the sticking coefficient is approximately unity and the sublimated flux takes into account any (indistinguishable) molecules that would be re-emitted from the frost surface. Molecules landing on a rock surface reside for a period of time dependent on T_s given by $t_{res} = \exp\left[\Delta H_s / k_B T_s\right] / \nu_o$ [15]. Here, ν_o is the lattice vibrational frequency of SO_2 within its surface matrix site, ΔH_s is the surface binding energy of SO_2 on its own frost, and k_B is the Boltzmann constant.

The simulation of Io's atmosphere is a weakly unsteady problem when planetary rotation and non-uniform frost coverage are included. A three step process is used to compute a quasi-steady state atmosphere. First, the temperature distributions of frost and rock are solved independently with no atmosphere present and then these temperature distributions are used to create a quasi-steady frost distribution on the rock as a result of simple free molecular flow. The steady state surface temperature distribution and frost boundary condition are then used to create a quasi-steady state atmosphere. Due to its high emissivity the rock surface temperature is essentially that of a surface in local radiative equilibrium with the solar flux. The frost surface temperature distribution showed significant thermal lag at the dusk terminator due to the low frost emissivity. The computed temperature distribution reached steady state after one Io rotation and the surface frost boundary condition reached steady state after half a rotation. The atmosphere equilibrates on a gas dynamic time scale much sooner (~20° of rotation).

The atmosphere was in steady state when the gas properties such as temperature and density were found to have only small time variations attributed to the slowly changing surface temperature and frost fraction. The convergence of the atmosphere to steady state was made more rapid by initially using a low number of representative molecules and allowing the atmosphere to equilibrate. The weighting function was then altered to clone all the molecules in the domain. The new atmosphere was then allowed to relax through collisions to a new steady state.

Since the density varies over five orders of magnitude, ~100 representative molecules in the cells with highest density would mean that many cells would on average have no molecules present. This necessitates the use of a weighting function. The weighting function adjusts the ratio of computational particles to real particles in every vertical column of cells based upon the surface area and temperature of the corresponding surface cell. The weighting function is chosen so that each surface cell will sublimate the same number of molecules (this boosts the number of molecules in the small cells near the poles) and such that the total number of molecules per processor is uniform.

In order to validate our atmospheric model, we compare spectra based on the atmospheric model with observed spectra of Io's atmosphere. The direct comparison of spectra is preferable to comparing model atmospheric properties with those deduced from the interpretations of the spectroscopic data. The latter approach always requires implicit assumptions to be made regarding the state of the atmosphere while the former requires none.

A 3-D radiative transfer model utilizing the backward Monte Carlo method was developed to model the atmospheric radiation. In this method photon bundles are traced in a time reversed manner from the detector toward the atmosphere, until they are absorbed by the planetary surface or gas. The major difference between the MC radiative transfer method and DSMC is that photons do not interact with each other, and therefore can be tracked independently through the computational grid. The backward method is ideal for modeling the radiation from an atmosphere observed by distant detectors with a narrow field of view. The theoretical basis for this method arises from (i) the principle of reciprocity in radiative transfer theory [16] and (ii) the fact that the probability of a photon traveling along a specific path is independent of the direction in which the path is followed. Details of the backward MC method as applied to the transfer of radiation in participating scattering medium are given by Walters and Buckius [17, 18].

Recently, Oikarinen et al. [19] developed a fully 3-D backward MC model for a spherical-shell atmosphere and applied it to the problem of limb-viewing measurements in order to extract the vertical composition of the Earth's atmosphere. Spada et al. [20] developed a fully 3-D backward model for spherical shell atmospheres to study intensity measurements in limb-viewing instruments. These models only predict the observations of sunlight reflected by the surface and/or scattered in the atmosphere, while our model also allows for volumetric emission within the atmosphere. This allows us to find not only solar UV/visible radiation scattered by the planetary atmosphere, but also IR and millimeter radiation emitted by the atmosphere itself.

In the backward MC method, the radiation intensity reaching the detector, $I_\lambda(\mathbf{r}_d, -\mathbf{\Omega}_d)$, can be found by emitting N photon bundles from the detector at the position $\mathbf{r}_d$ with direction $\mathbf{\Omega}_d$ into a scattering, absorbing, and non-emitting medium. Each photon bundle will trace a zig-zag trajectory, with scattering locations found from sampling of the scattering optical depth $\tau_\sigma = -\ln(1-R_\sigma)$, where R_σ is a uniformly distributed random number. If a photon bundle encounters the surface with reflectivity $\rho(\mathbf{r}_s)$, then it will be reflected with this probability. The

direction of a bundle following each scattering/reflection is found based on the scattering phase functions of a medium/surface at the point of interaction. The contribution of the *k*-th photon bundle to the specific intensity is given by [18]

$$I_\lambda^k(\mathbf{r}_d, -\hat{\Omega}_d) = I_{s\lambda}(\mathbf{r}_s)e^{-\tau_\lambda(0)} + \sum_{m=1}^{M} B_\lambda(T_m)\left(e^{-\tau_\lambda(l_{m2})} - e^{-\tau_\lambda(l_{m1})}\right), \tag{1.2}$$

where M is a total number of the volume cells traced by each bundle, $B_\lambda(T_m)$ is a thermal source in the m-th cell, $I_{s\lambda}(\mathbf{r}_s)$ is the surface intensity at the point where the bundle was absorbed, l_{m1} is the location of the cell edge along the zig-zag path closest to point of emission, while l_{m2} is the position of the cell edge closest to the detector. The optical depth entering the above equation is calculated based on the absorption coefficient κ_λ and is defined as

$$\tau_\lambda(l_*) = \int_{l_*}^{l_{TOA}} \kappa_\lambda(l'_*)dl'_* \tag{1.3}$$

Where l_* is measured from the point in the cell volume to the top of the atmosphere, l_{TOA}. The individual estimates of the specific intensity are then averaged for the N traced bundles.

If the wavelength of the radiation is such that the solar illumination contributes to the radiation observed by detector (UV/vis/nIR), then the internal source function $B_\lambda(T_m)$ and the surface brightness $I_{s\lambda}(\mathbf{r}_s)$ are adjusted to account for the scattering/reflection of collimated solar radiation. This method allows us to incorporate collimated radiation effectively as an additional anisotropic emission from the gas and the surface. If the medium is neither scattering nor reflecting the radiation, the formulation of the backward Monte Carlo method reduces to line-of-sight calculations.

RESULTS

The effects of the inhomogeneous surface frost model without (Case 1) and with (Case 2) a residence time on rock are examined (Fig. 1). Streamtraces for Case 1 show that the flow is not directly away from the subsolar point because of the inhomogeneous surface frost (or Monte Carlo noise). Local flows (~50 m/s) develop where strong frost gradients occur (especially on the night-side). Because the vapor pressure is exponentially dependent upon the surface temperature, the vapor pressure drops rapidly near the terminator. The pressure gradient from the subsolar point to the terminator is strong enough to drive the flow supersonic. A strong circumplanetary flow develops away from the subsolar point toward the terminator peaking at a Mach number of ~1.8 for Case 1 and ~1.6 for Case 2 both at an altitude of ~40 km. The region where the flow goes supersonic and is then decelerated by a standing shock can be seen bracketed by the thick black lines in Fig. 1.

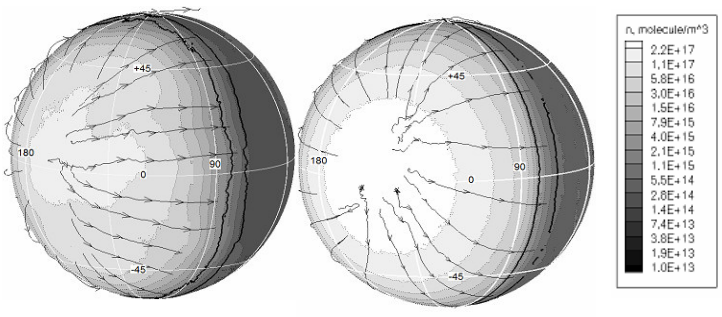

FIGURE 1. Number density contours at an altitude of 3 km with stream traces and the sonic line in thick black. (1a) shows Case 1, while (1b) shows Case 2.

In Case 1, where molecules stick to the rock, the flow goes supersonic at all latitudes on the dusk terminator whereas the flow at the dawn terminator (not seen) only goes sonic near the poles. The reason for the asymmetry in flow conditions for Case 1 is most likely that the dusk terminator is near the edge of a region of very low frost coverage. The low frost coverage leads to a low gas density and pressure which enhances the pressure gradient between the subsolar point and the terminator. In Case 2, the flow goes supersonic at all latitudes on both terminators. The reason for the flow differences between Cases 1 and 2 is that in Case 2 the hot rock smoothes gas density by quickly re-emitting the fraction of gas that falls on the rock surface. This smoothes the inhomogeneities caused by the surface frost distribution in Case 1.

The column density in Case 1 is found to be controlled principally by the surface temperature, with the surface frost coverage having a small but noticeable effect. The inhomogeneity in column densities caused by the surface frost coverage is seen most strongly near the subsolar point where the temperature gradient is the weakest. Circumplanetary flow does not significantly alter the column densities from hydrostatic equilibrium in either case, with the exception of the area near the dawn terminator in Case 2. The exponential dependence of the vapor pressure on T_s and hence sublimated flux of SO_2 explains the dominant effect of T_s on the column density. The surface frost coverage has only a linear effect. In Case 2, the surface frost coverage has a negligible effect on the column density.

The presence of hot rock that re-emits molecules that fall upon it after only a few seconds acts to homogenize the column density contours to very nearly follow the surface temperature.

The vibrational temperature is highly non-equilibrium at all mid to high altitudes. In Fig. 2b, contours of the vibrational temperature in the ν_2 band are shown for a cross-sectional slice of Io's atmosphere along the equator. The vibrational temperature is derived from the ratio of the number of molecules in the first excited state to the number in the ground state. The night-side is weakly populated at all longitudes and altitudes and there are nearly zero vibrationally excited SO_2 molecules above an altitude of ~50 km leading to zero vibrational temperature. The two mechanisms which can vibrationally excite an SO_2 molecule are intermolecular collisions and sublimation from the surface (since the molecule is assumed to be in thermal equilibrium with the surface). The vibrational de-excitation of an SO_2 molecule occurs rapidly for the ν_2 band. Nearly everywhere in the atmosphere, the de-excitation rate ($A_{1\text{-}0,\nu_2} = 44\ \mathrm{s}^{-1}$) is faster than the mean time between collisions. Therefore, near the surface the vibrational temperature is in equilibrium with the rotational and translational temperature, but rapidly becomes non-equilibrium with increasing altitude. The plasma heating causes the vibrational temperature to increase above an altitude of 5 km near the subsolar point. Below 5 km, the plasma energy is completely depleted due to the dense column of gas. Although the plasma energy does not directly excite the ν_2 band of SO_2, it does increase the translational energy of SO_2 molecules which can lead to more energetic collisions and more likely vibrational excitation.

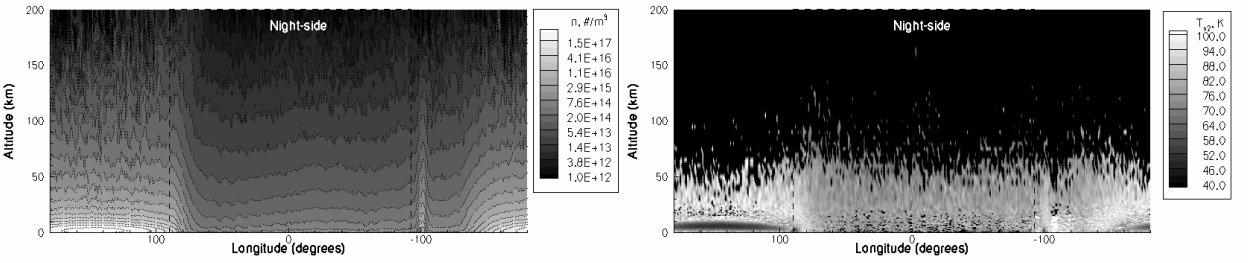

FIGURE 2. Contours of (a) number density and (b) vibrational temperature for a cross-sectional slice through the equator for Case 2 are shown. The vibrational temperature is zero above ~50 km due to inadequate statistics.

The gas density can be vertically integrated to yield the vertical column density that can be compared to results derived by Feaga [10] and Spencer et al. [21]. Spencer et al. found that for the modified latitude model which best fit the data, the peak equatorial vertical column density was ~1.5×10^{17} cm^{-2} which matches well with the peak value of our model for Case 1 [21]. Feaga's [10] column densities are an average day-side vertical column density. This represents the average of many different orbital longitudes, whereas our model column density represents the column for single subsolar longitude. Since the effects of circumplanetary flow and inhomogeneous surface frost have been found to have only a small effect on the vertical column density, an analytic day-side average vertical column density can be calculated by assuming that the temperature varies only with latitude. The average dayside column densities (not shown) have a banded structure similar in morphology to those derived by Feaga [10]. However, Feaga's column densities drop at lower latitudes and much more sharply than our analytic column densities. For Case 1, the peak column density was found to be ~1.5×10^{17} cm^{-2} which is over twice as large as the value of 5.0×10^{16} cm^{-2} derived by Feaga [10]. For Case 2, the peak column density is found to be ~3.2×10^{17} cm^{-2}. The discrepancy in column density can be explained by a very small difference (~2 K for Case 1 and ~4 K for Case 2) in the subsolar temperature used in our model because the column density is exponentially dependent on the surface temperature.

We apply the radiative transfer model to predict the radiation arriving at an Earth-based detector from the atmosphere of Io in the narrow wavenumber range 530.35-530.45 cm^{-1} of the ν_2 vibrational band of SO_2. The spectral range chosen corresponds to the observations of Spencer at al., [21] who detected SO_2 absorption spectra in the ν_2 band over the sunlit hemisphere of Io during the years 2001-2005. The absorption coefficient of the SO_2 gas is calculated using a line-by-line method, utilizing the line parameters from the Flaud et al. [22] Surface frost emissivities of SO_2 and S (for the rock) are from Nash and Betts [23] and Nash [24], who obtained the laboratory mid-infrared spectra of these materials. The reported values of reflectivity at 530.4 cm^{-1} are unity for the SO_2 frost and 0.8 for the S frost. The relative fraction of the two surface materials is obtained from the NIMS data [9]. The non-LTE state of the atmosphere in the model is accounted for by using the vibrational temperature T_{vib} instead of the kinetic temperature to calculate the vibrational partition sum and the Planck blackbody function.

In accordance with the observational data, we calculated the band depth of the strongest feature in the spectrum centered at 530.42 cm^{-1} at zero phase angle. The band depth is a measure of the atmospheric absorption and self emission of the radiation and is defined as $(I_c - I_{bc})/I_c$, where I_c is a continuum specific intensity from the surface, and

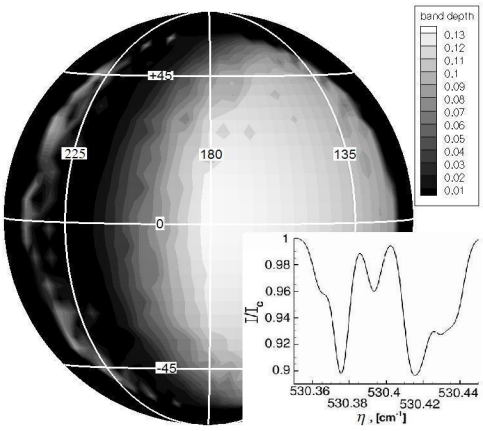

FIGURE 3. Contours of the band depth of the strongest feature in the spectrum of the atmosphere. (Inset) Disk integrated band depth of the atmosphere.

I_{bc} is the specific intensity measured in the band center. Figure 3 shows the disk resolved band depth for a central longitude of 180° and indicates a much stronger absorption in the visible part of the Eastern hemisphere (90°-180°). The atmosphere far to the west of the subsolar point (~250°-270°) has not yet developed, as a result of thermal inertia of ground, while the atmosphere east of the subsolar point (~70°-90°) has not yet collapsed. Thus the region of the maximum column density will always lie to the east of the subsolar point, which is also clear from the contours of number density on Fig. 2a. In the visible part of the western hemisphere (180°-270°) the band depth decreases monotonically until the sudden jump near the limb where the air mass increases as a result of the spherical geometry, producing higher column density and stronger atmospheric absorption. The part of the disk near the limb without underlying surface has zero band depth, as it does not contain underlying continuum radiation. Figure 3 (inset) shows the disk integrated spectrum of the atmosphere normalized to the continuum. The disk integrated band depth of the strongest feature is ~10%. The shape of the band is identical to the one observed by Spencer et al. [21, Fig. 13], however the observation resulted in a lower band depth of ~7%. The disagreement may result from the difference in the column densities and/or the vertical temperature profiles between the observed and simulated atmospheres, and is a subject of the ongoing investigation. As the investigation of the immediate source (sublimation/volcanic) of the atmosphere on Io continues, future space probes may measure disk resolved band depth of the atmosphere. Finding the lag in the band depth with respect to the subsolar point will serve as a strong indicator toward the sublimation model.

ACKNOWLEDGEMENTS

NASA Planetary Atmospheres Grant, NNG05G083G, funded this research. Computations were done at the Texas Advanced Computing Center.

REFERENCES

1. J. Saur and D. F. Strobel, *Icarus* **171**, 411-420 (2004).
2. A. Ingersoll, M. Summers, S. Schlipf, *Icarus* **64**, 375-390 (1985).
3. M. Moreno, G. Schubert, J. Baumgardner, M. Kivelson, D. Paige, *Icarus* **93**, 63-81 (1991).
4. M. Wong and R. Johnson, *Icarus* **115**, 109-118 (1995).
5. M. Wong and R. Johnson, *J. Geophysical Res.* **101**, 23243-23254 (1996a).
6. M. Wong and W. Smyth, *Icarus* **146**, 60-74 (2000).
7. M. Pospieszalska and R. Johnson, *J. Geophysical Res.* **101**, 7565-7573 (1996).
8. J. Austin and D. Goldstein, *Icarus* **148**, 370-383 (2000).
9. S. Douté, B. Schmitt, R. Lopes-Gautier, R. Carlson, L. Soderblom, J. Shirley, Galileo NIMS, *Icarus* **149**, 107-132 (2001).
10. L. Feaga, Hubble Space Telescope Far-Ultraviolet Observations of Io: Determing Atmospheric Abundances, Mapping the SO_2 Distribution, and Correlating the Molecular and Atomic Atmosphere. PhD Dissertation. Johns Hopkins Univ. 2005.
11. G. Bird, *Molecular Gas Dynamics and the Direct Simulation of Gas Flows*. Oxford Univ. Press. Oxford, 1994.
12. J. Zhang, D. Goldstein, P. Varghese, N. Gimelshein, S. Gimelshein, and D. Levin, *Icarus* **163**, 182-197 (2003).
13. D. Wagman, Sublimation pressure and the enthalpy of SO_2. Chem. Thermodyn. Data Cent., Natl. Bur. of Stand. (1979).
14. J. Rathbun, J. Spencer, L. Tamppari, T. Martin, L. Barnard, and L. Travis, *Icarus* **169**, 127-139 (2004).
15. S. Sandford and L.J. Allamandola, *Icarus* **106**, 478-488 (1993).
16. K. Case, *Review of Modern Physics*, Vol. **29**, pp. 651-663 (1957).
17. D. V. Walters, R. O. Buckius, *Annual Review of Heat Transfer* **5**, Hemisphere, New York, 131-176 (1992a).
18. D. V. Walters, R. O. Buckius, *International Journal of Heat and Mass Transfer* **35**, 3323-3333 (1992b).
19. L. Oikarinen, E. Sihvola, E. Kyrölä, *J. Geophysical Res.* **104**, 31261-31274 (1999).
20. F. Spada, M. Krol, P. Stammes, *Atmos. Chem. Phys.* **6**, 4823-4842 (2006).
21. J. Spencer, E. Lellouch, M. Richter, M. Lopez-Valverde, K. Jessup, T. Greathouse, J. Flaud, *Icarus* **176**, 283-304 (2005).
22. J. Flaud, A. Perrin, L. Salah, W. Lafferty, G. Guelachvili, *J. Molecular Spectroscopy* **160**, 272–278 (1993).
23. D. Nash, B. Betts, *Icarus* **117**, 402–419 (1995).
24. D. Nash, *Applied Optics* **25**, 2427-2433 (1986).